J Electr Eng Technol.2018; 13(6): 2434-2440
http://doi.org/10.5370/JEET.2018.13.6.2434

ISSN(Print) 1975-0102
ISSN(Online) 2093-7423

Development of High Frequency pMUT Based on Sputtered PZT

Un-Hyun Lim*, Jin-Hee Yoo*, Vijay Kondalkar* and Keekeun Lee†

Abstract – A new type of piezoelectric micromachined ultrasonic transducer (pMUT) with high resonant frequency was developed by using a thin lead zirconate titanate (PZT) as an insulation layer on a floating 10 μm silicon membrane. The PZT insulation layer facilitated acoustic impedance matching at active pMUT, leading to a high performance in the acoustic conversion property compared with the transducer using SiO_2 insulation layer. The fabricated ultrasonic devices were wirelessly measured by connecting two identical acoustic transducers to two separate ports in a single network analyzer simultaneously. The acoustic wave emitted from a transducer induced a 3.16 μW on the other side of the transducer at a distance of 2 cm. The transducer performances in terms of device diameters, PZT thickness, annealings, and different DC polings, etc. were investigated. COMSOL simulation was also performed to predict the device performances prior to fabrication. Based on the COMSOL simulation, the device was fabricated and the results were compared.

Keywords: Ultrasonic transducer, pMUT, PZT, High resonant frequency, COMSOL.

1. Introduction

Ultrasonic transducers are widely used in a variety of applications including medical imaging, cellular stimulation, sonar, non-destructive tests, and distance measuring sensors. Recently, various configurations of pMUT and capacitive micromachined ultrasound transducer (cMUT) have been reported using the latest micro electro-mechanical system (MEMS) technologies [1-5] but most of the pMUTs and cMUTs have been fabricated on a SiO_2 insulation layer [6-8]. The cMUT requires a small gap between layers and a very strong bias voltage. However, the pMUT oscillates ultrasonic waves easily using piezoelectric materials, and high sensitivity is obtained even with a low bias voltage. The pMUT is more suitable for achieving high sensitivity and high frequency characteristics in the GHz range. The pMUT frequency band is determined according to the transducer structures and the material properties as shown in the following Eqs. [9].

$$\text{Frequency} = \frac{\alpha}{2\pi r^2}\sqrt{\frac{D_E}{\rho h}} \quad \text{and} \quad \mathrm{D_E} = \frac{Eh^3}{12(1-v^2)} \qquad (1)$$

Here, α is the resonance mode constant, r the radius of the diaphragm, D_E the flexural rigidity, ρ the effective density of the diaphragm, h the diaphragm thickness, E the effective Young's modulus, and v the Poisson's ratio. The piezoelectric material in the pMUT has the largest influence on the performance. In present MEMS technology, aluminum nitride (AlN) and PZT are widely used for the pMUT. In particular, PZT is known as a material that has a large piezoelectric constant (d_{31}) in the flexural mode and a small dielectric loss, and thus is the most widely used in the pMUT technology [10-12]. N. Hanajima et. al. developed a sol-gel PZT piezoelectric membrane actuator with a 1.75 GHz band and analyzed by the S-parameter to confirm the resonant frequency [13]. H. Lobl et. al. demonstrated a two-port band-pass filter using PZT, and proposed an efficient DC poling method for polarization and then verified the performances [14]. Generally, a SiO_2 insulating layer is primarily used as the substrate when fabricating the pMUT [15]. However, PZT and SiO_2 have a large difference in the lattice constant, and the acoustic impedance mismatch between PZT and SiO_2 may greatly affect the wave properties when a high-frequency acoustic wave radiates.

To improve the performance of the ultrasonic transducer in the UHF band, we newly inserted a thin PZT layer on a floating 10 μm silicon membrane as an insulation layer for better oscillation. PZT has a relatively high resistivity of a ~2.88×10^8 ohm-cm, so that it performs well its insulation performance up to high frequency. When the ultrasonic wave radiates into the air, acoustic impedance matching should also be considered between layers to obtain a maximum radiation efficiency. The PZT insulation layer is so beneficial to obtain the acoustic impedance matching between layers owing to a smaller difference of the acoustic resistance. Above all, PZT has face center cubic (FCC) based unit cell, the same as the used metal, so that a stress effect caused by lattice mismatching between layers is minimized. Two different devices with SiO_2 and PZT insulation layer were experimentally fabricated in this paper and then their results were compared and analyzed. Furthermore, the resonant frequencies in terms of the radius of the piezoelectric element were checked, and the

† Corresponding Author: Dept. of Electrical and Computer Engineering, Ajou University, Korea. (keekeun@ajou.ac.kr)
* Dept. of Electrical and Computer Engineering, Ajou University, Korea. (keekeun@ajou.ac.kr)
Received: April 12, 2018; Accepted: July 9, 2018

Copyright ⓒ The Korean Institute of Electrical Engineers
This is an Open-Access article distributed under the terms of the Creative Commons Attribution Non-Commercial License (http://creativecommons.org/licenses/by-nc/3.0/) which permits unrestricted non-commercial use, distribution, and reproduction in any medium, provided the original work is properly cited.

ultrasonic transmissions were analyzed by connecting two identical devices to two separate ports in a single network analyzer simultaneously.

2. Optimal Design and Simulation

Fig. 1 shows the schematic view of the fabricated ultrasonic transmitter. A 1 μm thick PZT layer was placed on a silicon wafer as an insulation layer for better oscillation, and then Cr electrode was formed on the top of the PZT enhancer layer. The composition ratio of lead zirconate titanate $Pb(Zr_xTi_{1-x})O_3$ was 0.52 in x [16]. Next, another PZT layer and a top Cr electrode were formed. The device was circular to focus the wave, and the radius was varied from 0.5~4 mm. After completing the top devices, the bottom silicon was etched away, leaving only the 10 μm thick silicon for the flexural mode and for minimizing the parasitic capacitance effect.

A COMSOL simulation was performed to predict the resonant frequency of our designed structure and the ultrasonic propagation into the air. For the FEM simulation, the acoustic-piezoelectric interaction and frequency material system were employed in the COMSOL Multiphysics. The boundary medium was set to air to check the amount of energy propagated into the air. Overall device configuration and dimensions are the same as that of the actually fabricated device. PZT-5H with the same characteristics as the $Pb(Zr_{0.52}Ti_{0.48})O_3$ material was employed as the piezoelectric material and the electrode metal was chosen as Cr. Fig. 2 shows the simulated sound wave into the air in terms of the 3-D beam profile and the vertical distance, in which the diameter of the element set was 1 mm. For our designed parameters, the resonant frequency appears at approximately 1.7 GHz. Owing to the high frequency radiation, pressure signal attenuation occurs within a few millimeters when propagating into the air as shown in Fig. 2(b). The simulated ultrasonic wave is longitudinal pressure wave. The pressure wave consists of a repeating pattern of high-pressure and low-pressure regions moving through a medium. As shown in Fig. 2(b), the pressure level are varied periodically and constantly to make a propagation of the wave through air.

The attenuation of ultrasonic waves radiating into the air varies considerably depending on the distance measured,

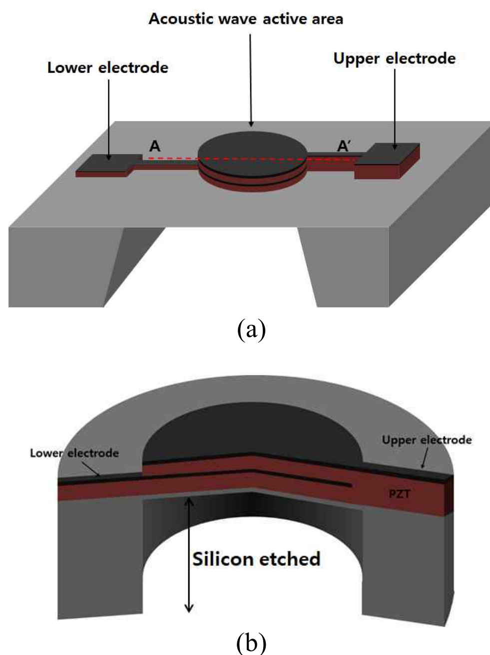

Fig. 1. 3D schematic view of piezoelectric membrane transducer: (a) Entire view and (b) cross-sectional view of the cut A-A'

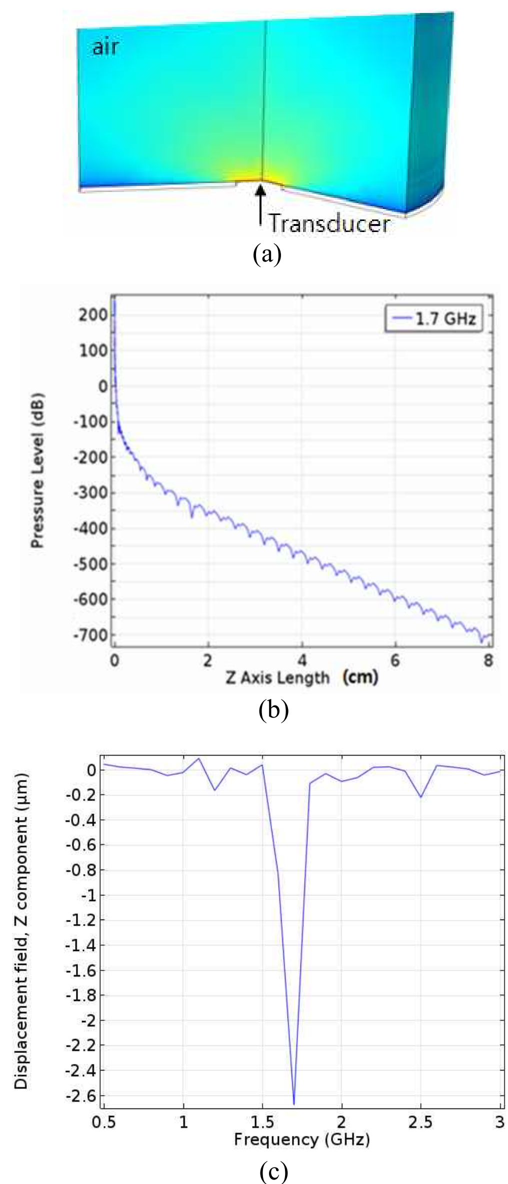

Fig. 2. COMSOL simulation results (a) for beam profiling over the air, (b) pressure levels in terms of distance, and (c) amplitude displacement of the membrane in z axis in terms of frequency

and depends on the center frequency used. Here, the attenuation means a reduced amplitude in the ultrasonic wave. The causes for the attenuation were beam spreading, absorption by particles in the air, dispersion, nonlinearity, scatterings by inclusions, etc. For the delivery of ultrasound with high frequencies in the air, the initial amplitude must generally be large and have low attenuation constants. Fig. 2(c) shows the simulated sound wave into the air in terms of the z-displacement in the vertical distance. The membrane oscillates with the highest amplitude at a ~1.7 GHz, which is the resonance frequency in the simulation configuration.

To minimize the attenuation of the ultrasonic wave, our measurement was performed under a clean and dry environment at room temperature. From the device perspective, the silicon substrate underneath the membrane was removed, leaving only 10 μm in thickness for the flexural mode and for minimizing the parasitic capacitance interference effect. Additionally, a thin PZT enhancer layer was added to the bottom layer to increase the ultrasonic amplitude at low actuation voltage, and the residual stress of the membrane and mass loading effect were minimized.

3. Fabrication and Poling Process

Fig. 3 describes the fabrication process of the device. First, a thick photoresist (AZ P4620) was patterned on the substrate for the lift-off process, and then PZT in the sputtering system and Cr in the e-beam evaporator were deposited, followed by the PR being dissolved in acetone. The PR was not damaged during the sputtering process, and was dissolved well in acetone. The bottom PZT layer is used as an insulating and enhancer layer. Next, the same process was repeated for the additional PZT and Cr layers. Some overlap occurs between the two PZT layers. However, the two metal electrodes were completely separated, as shown in Fig. 1(b). The top electrode and the underlying PZT layers were designed to protrude slightly to eliminate the step problem during fabrication. The relevant deposition condition for PZT is important because the quality of the PZT layer depends on sputtering conditions such as temperature, power, and pressure [17]. Typically, the higher the temperature, the higher is the deposition rate, but the pressure and power also affect the composition ratio of PZT [18-19].

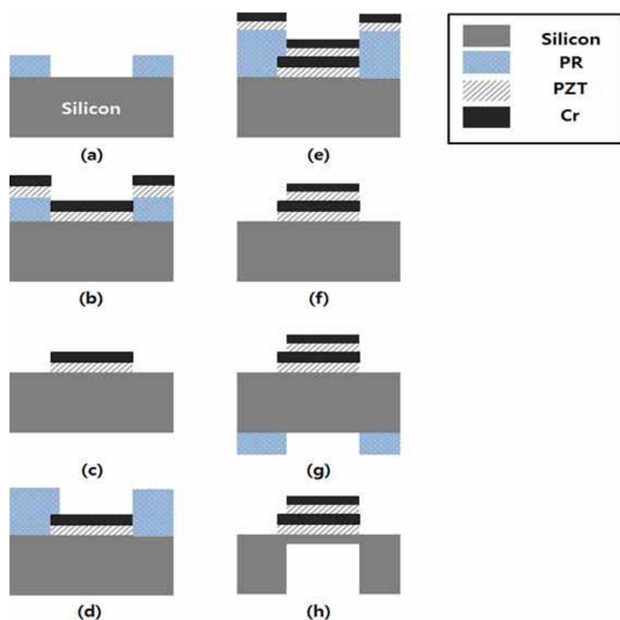

Fig. 3. Schematic of fabrication process. (a) Si substrate patterned by photoresist, (b) deposition of PZT-Cr layer, (c) lift-off by acetone, (d) PR photolithography, (e) active PZT, ground electrode deposition, (f) PR lift-off, (g) backside alignment for silicon etching, and (h) silicon DRIE

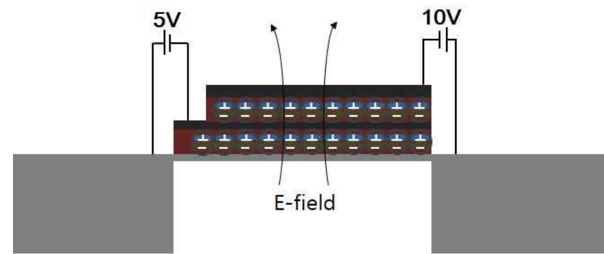

Fig. 4. Cross-sectional view of DC re-poling process. A 5kV/cm field was applied to each PZT layer

After completing the top devices, the bottom silicon was etched using a ~20 μm thick PR (AZ 4620) as a protective layer on the backside of the silicon. The thicknesses of the PR (AZ4620) and silicon were 20 μm and 500 μm, respectively. The PR had performed its masking role well during DRIE process. The calculated PR:Si selectivity was over 1:50. The etch time and etch rate were carefully monitored and controlled to leave approximately 10 μm of silicon underneath the device. After PZT was deposited, post-annealing and DC poling were performed. Post-annealing was carried out at 650°C using the RTA system after heating the device at 300°C on a hot plate [20]. The DC poling process was performed on a 120 °C hot plate by applying a 5 kV/cm field as shown in Fig. 4, in which two PZT layers are poled simultaneously in the same direction.

4. Results

4.1 Fabricated device

The fabricated devices were viewed using an optical microscope and SEM. Fig. 5 shows the top, cross-sectional, and bottom views of the fabricated device. The device was circular and well-patterned, and the diameter of the circular was ~1 mm. As shown in Fig. 5(b), only 10 μm of silicon remained in the membrane, and the rest of the silicon was etched away. The PZT thickness was ~1 μm. Fig. 6 shows the XRD patterns of PZT under the condition of Cr in the

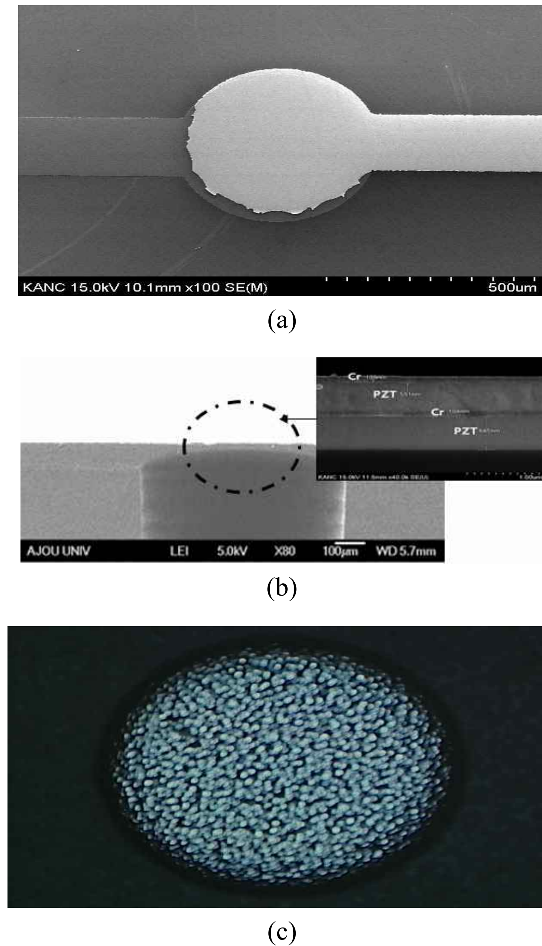

(a)

(b)

(c)

Fig. 5. SEM and optical views of the fabricated pMUT. (a) Top view and (b) cross-sectional and magnified views of the membrane. (c) Optical view of the etched silicon taken from bottom side

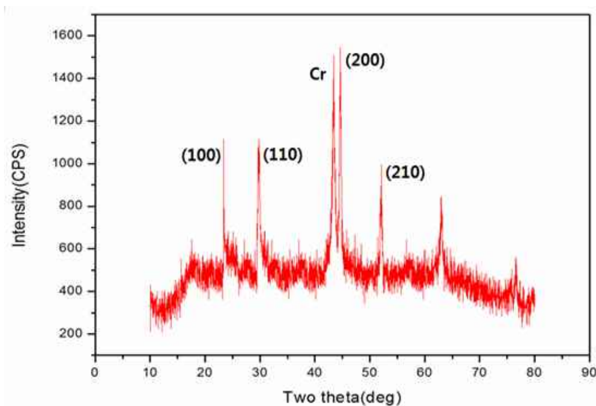

Fig. 6. XRD pattern after removing the top metal electrode, showing clear peaks at (100), (110), and (200) planes

middle and the absence of the top electrode metal. The XRD pattern provided the peaks from the (100), (110), and (200) planes. The peaks are clearly shown as predicted, confirming a high quality PZT layer.

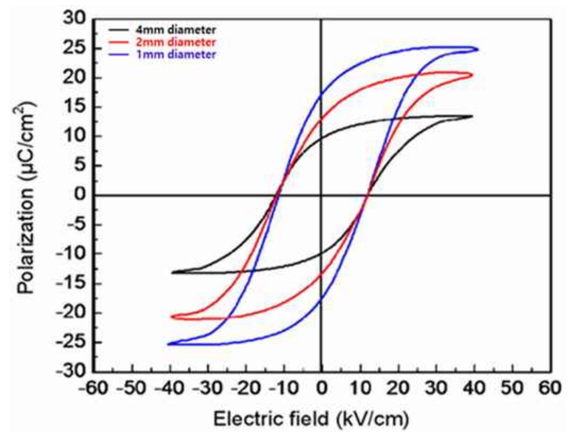

Fig. 7. Hysteresis loops from the devices with various radius. Polarization slope is sharp when diameter of the device is smaller

4.2 Hysteresis loop characterization

The degree of polarization in our device operating as the d_{31} mode varies with the diameter of the device [21]. The threshold voltage (the voltage at which the left and right hysteresis loops disappear in Fig. 7) of the hysteresis loop does not change because the threshold voltage is only determined by the thickness of the ferroelectric material between two electrodes. That is, in our d_{31} flexural mode, the degree of polarization varies with the diameter of the device rather than the thickness of the device. Fig. 7 shows a hysteresis loop of the devices with diameters of 1 mm, 2 mm, and 4 mm. The threshold voltage is 4.5 kV/cm for all three devices, but the polarizations are different at the zero point, i.e., 10 μC/cm^2, 13 μC/cm^2, and 17 μC/cm^2, respectively. As shown from this hysteresis measurement, when DC re-poling is performed, a 5 V voltage is to be applied in consideration of the PZT thickness (~1 μm) between two electrodes. Applying a voltage of 5V or higher may increase the polarization and the operating lifetime of the device, but the connection pads can be torn because of a high E-field induction.

4.3 Resonant frequency analysis

To obtain the resonant frequency of the completed device, the device was wire-bonded to the PCB substrate and the S_{11} was analyzed on the HP 8510 network analyzer. Fig. 8 compares the resonant frequencies of three devices, i.e., a device fabricated on a quartz wafer (SiO_2 bulk), a device using SiO_2 as an insulating layer (without PZT), and a device using a PZT layer as an insulating layer. The minimum point of the S_{11} is considered as the resonant frequency. The frequency was swept, and S_{11} was monitored. As shown in Fig. 8, the resonant frequency of the device fabricated on the PZT insulation layer onto a thin silicon membrane was 1.68 GHz, and the device fabricated on a PZT insulation layer onto a quartz bulk wafer shows a

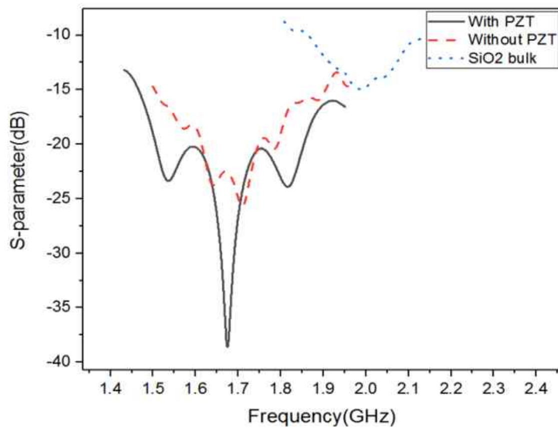

Fig. 8. Comparisons of the resonance frequencies from three different transducers

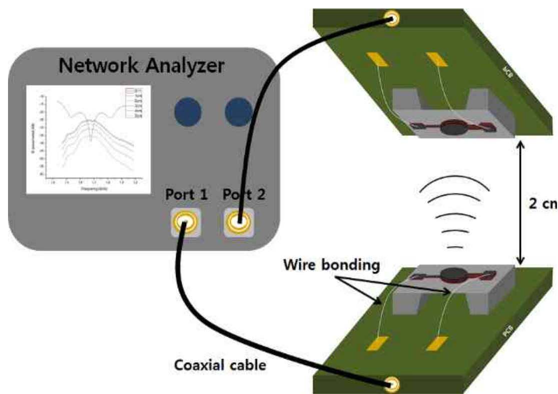

Fig. 9. Schematic of testing setup. Two identical transducers were connected to two ports simultaneously in the network analyzer to verify ultrasound wave transmission

resonant frequency at 2.0 GHz. For the device fabricated on a quartz wafer, the resonant frequency is up-shifted to a higher frequency owing to the bulk thickness. In addition, the minimum values in S_{11} show a large difference, -15 dB for quartz-based devices, and -37 dB for devices with a PZT insulation layer on a thin silicon membrane. The minimum value is an indicator of the amount of electrical energy that is converted into pressure to radiate into the air. The transducer fabricated on the thin membrane showed a low resonant frequency and high acoustic conversion efficiency. Fig. 9 shows a schematic of the wireless testing setup. Two identical devices are simultaneously connected to two ports of the network analyzer.

An electrical energy is applied to port 1, and a pressure wave is transmitted through the transducer in port 1 to the device connected to port 2. The transducer of port 2, which receives the pressure wave, converts again to electrical energy and then provides the signal of S_{12}. Additionally, S_{12} is a parameter that can be used to determine the amount of electrical energy entering port 2 by receiving a pressure wave. No electrical energy was applied to port 2. As

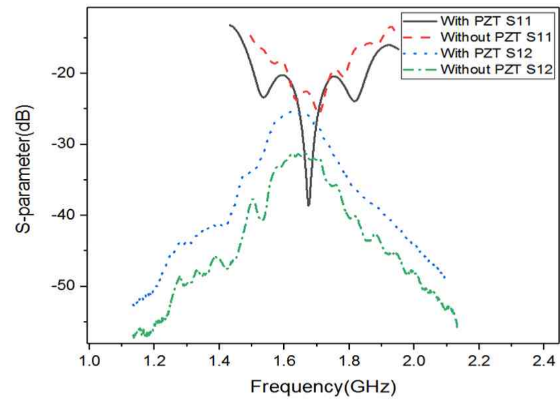

Fig. 10. Ultrasound transmission analysis by S-parameters S_{11} and S_{12}

acoustic energy is delivered to port 2 from port 1, the acoustic energy is converted to electrical energy at port 2 and then expressed in S_{12} (dB) based on 1 mW.

Fig. 10 shows the results of S_{11} of the device connected to port 1, and S_{12} of the device receiving the pressure wave at port 2. The transducer with the PZT insulation layer on the silicon membrane and the transducer on the SiO_2 bulk wafer were compared. Unlike a function generator, a network analyzer cannot emit a specific frequency; therefore, the signals are difficult to measure accurately. However, a network analyzer is a very useful tool to examine an acoustic transmission process, in which a transducer emits an acoustic wave and converts it to electrical energy after receiving the emitted acoustic wave. As shown in Fig. 10, all devices responded to the signals in the resonant frequency band. All devices were measured at the same distance from each other. The peak point of the device with the PZT insulation layer on silicon membrane is -25 dB and the peak point of the device with the SiO_2 insulation layer is -32 dB in the S_{12}.

The higher the S_{12} peak point, the greater the electrical energy entering port 2, proving that the device with the PZT insulation layer provides more pressure waves in the resonant frequency band. Here, the S_{12} values were somewhat slow-sloped and different from the S_{11} shapes around the resonant frequency. For these reasons, we consider that the transducer at port 1 receives 1 mW of electrical energy from the network analyzer directly and then emits ultrasonic waves at all frequency bands, but have a maximum signal emission at the resonant frequency. In contrast, the transducer in port 2 did not receive any electrical pulses, but it was actuated by both ultrasonic waves from port 1 and the surrounding interference noise waves, leading to a smooth slope in S_{12}. We can also calculate the amount of power delivered to the transducer at port 2. Since S_{12} obtained at port 2 was -25 dB and the reference power was 1 mW, the net power received by the transducer at port 2 was 3.16 μW. From these results, we confirmed that as the PZT buffer layer was inserted underneath the bottom metal electrode, a larger amplitude

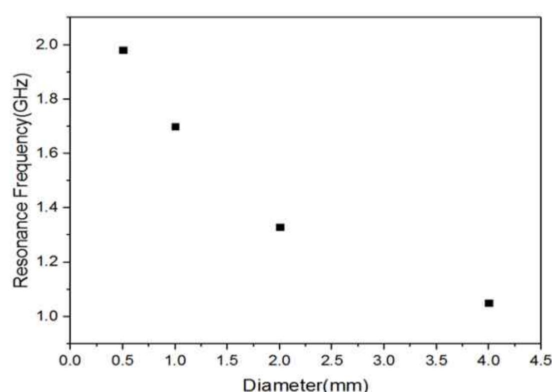

Fig. 11. Resonance frequency changes by diameters of the device

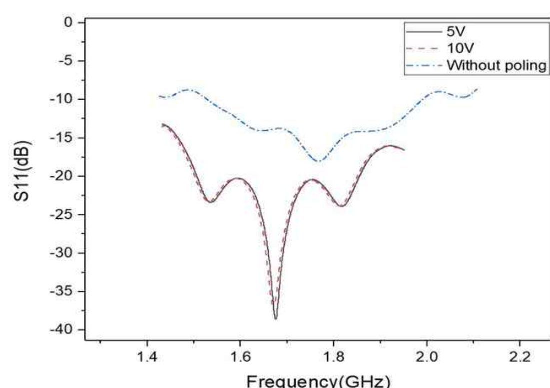

Fig. 12. DC poling effect on piezoelectric transducer

of the acoustic wave was obtained, enhancing energy conversion efficiency of the upper PZT layer. Fig. 11 shows the change in the resonant frequency in terms of the radius of the device. The larger the radius, the lower is the resonant frequency, as predicted in Eq. (1) and the COMSOL simulations.

4.4 Poling effect

The performance of the piezoelectric material varies depending on the poling degree. Fig. 12 compares the emitting powers of the acoustic wave from the transducers in terms of the DC voltage applied during the poling process. The device with no DC voltage applied showed a poor and low S-parameter performance. The devices with 5 V and 10 V applied during the poling process showed very high S_{11} parameter characteristics, confirming that complete poling occurs above 5 V in our device configuration, as suggested in the hysteresis loop measurement.

5. Conclusion

We have developed a pMUT device operable in the HF band by employing a thin PZT insulating layer underneath the bottom electrode. The transducer using PZT as an insulation layer provided better characteristics of S_{11} and S_{21}, because of an improved acoustic impedance matching and a minimal lattice mismatching between the layers. The silicon substrate underneath the transducer was removed for the flexural mode and for minimal parasitic capacitance. The PZT thickness of 1 μm and the radius of 1 mm provided the resonant frequency of 1.7 GHz. The developed transducer induced 3.16 μW of energy at a distance of 2 cm.

Acknowledgements

This research work supported by the Korea Institute of Energy Technology Evaluation and Planning (KETEP) (Grant number: 20172220200110).

References

[1] J. Bernstein, S. Finberg, K. Houston, L. Niles, H. Chen, L. Cross, K. Li, and K. Udayakumar, “Micromachined high frequency ferroelectric sonar transducers,” *IEEE Trans. Ultrason. Ferroelect. Freq. Contr.*, vol. 44, pp. 960-969, Sept. 1997.

[2] I. Wygant, N. Jamal, and H. Lee, “An integrated circuit with transmit beamforming flip-chip bonded to a 2-D CMUT array for 3-D ultrasound imaging,” *IEEE Trans. Ultrason. Ferroelect. Freq. Contr.*, vol. 56, pp. 2145-2156, Oct. 2009.

[3] B. Khuri-Yakub and O. Oralkan, “Capacitive micro-machined ultrasonic transducers for medical imaging and therapy,” *J. Micromech. Microeng.*, vol. 21, pp. 054004, Mar. 2011.

[4] A. Hajati, D. Latev, D. Gardner, A. Hajati, D. Imai, M. Torrey, and M. Schoeppler, “Three-dimensional micro electromechanical system piezoelectric ultra-sound transducer,” *Appl. Phys. Lett.*, vol. 101, pp. 253101, Dec. 2012.

[5] Y. Qiu, J. Gigliotti, M. Wallace, F. Griggio, C. Demore, S. Cochran, and S. Trolier-McKinstry, “Piezoelectric Micromachined Ultrasound Transducer (PMUT) Arrays for Integrated Sensing Actuation and Imaging,” *Sensors*, vol. 15, pp. 8020-8041, Apr. 2015.

[6] M. Sherar and F. Foster, “The design and fabrication of high frequency transducer,” *Ultrasonic imaging*, vol. 11, pp. 75-94, 1989.

[7] T. Pedersen, T. Zawada, K. Hansen, R. Lou-Moeller, and E. Thomsen, “Fabrication of high-frequency pMUT arrays on silicon substrates,” *IEEE Trans. Ultrason. Ferroelect. Freq. Contr.*, vol. 57, pp. 1470-1477, June 2010.

[8] P. Kirby, Q. Su, E. Kornuro, Q. Zhang, M. Imura, and R. Whatmore, “PZT thin film bulk acoustic wave

resonators and filters," *presented at the IEEE Int. Conf. Frequency Control Symposium and PDA Exhibition*, 2001, pp. 687.

[9] A. Jakob, M. Bender, T. Knoll, R. Lemor, T. Lehnert, M. Koch, M.Veith, Q. Zhou, B. P. Zhu, J. X. Han, and K. K. Shung, "Comparison of different piezoelectric materials for GHz acoustic microscopy transducers," *presented at the IEEE Int. Ultrasonics Symposium*, 2009, pp. 1722-1725.

[10] T. Haccart, E. Cattan, and D. Remiens, "Dielectric, ferroelectric and piezoelectric properties of sputtered PZT thin films on Si substrates: influence of film thickness and orientation Semiconductor Physics," *Quantum Electronics & Optoelectronics*, vol. 5, pp. 78-88, 2002.

[11] L. Gabriel, J. Pulskamp, L. Sanchez, D. Potrepka, R. Proie, T. Ivanov, R. Rudy, W. Nothwang, S. Bedair, C. Meyer, and R. Polcawich, "PZT-Based Piezoelectric MEMS Technology," *J. Am. Ceram. Soc*., vol. 95, pp. 1777-1792, 2012.

[12] P. Muralt, N. Ledermann, J. Baborowski, A. Barzegar, S. Gentil, B. Belgacem, S. Petitgrand, A. Bosseboeuf, and N. Setter, "Piezoelectric micromachined ultrasonic transducers based on PZT thin films," *IEEE Trans. Ultrason. Ferroelect. Freq. Contr*., vol. 52, pp. 2276-2288, Dec. 2005.

[13] N. Hanajima, S. Tsutsumi, T. Yonezawa, and K. Hashimoto, "Ultrasonic Properties of Lead Zirconate Titanate Thin films in UHF-SHF Range," *Jpn. J. Appl. Phys*., vol. 36, pp. 6069-6072, Sept. 1997.

[14] H. Lobl, M. Klee, R. Milsom, R. Dekker, C. Metzmacher, W. Brand, and P. Lok, "Materials for bulk acoustic wave (BAW) resonators and filters," *J. Eur. Ceram. Soc*., vol. 21, pp. 2633-2640, 2001.

[15] G. Velu, D. Remiens, and B. Thierry, "Ferroelectric Properties of PZT Thin Films Prepared by Sputtering with Stoichiometric Single Oxide Target: Comparison Between Conventional and Rapid Thermal Annealing," *J. Eur. Ceram. Soc*., vol. 17, pp. 1749-1755, Feb. 1997.

[16] P. Muralt, A. Kholkin, M. Kohli, and T. Maeder, "Piezoelectric actuation of PZT thin-film diaphragms at static and resonant Conditions," *Sens. Actuators A*, vol. 53, pp. 398-404, 1996.

[17] I. Kanno, S. hayashi, T. Kamada, M. Kitagawa, and T. Hirao, "Low Temperature Preparation of Pb(Zr, Ti)O_3 Thin Films on (Pb, La)TiO_3 Buffer Layer by Multi-Ion-Beam Sputtering," *Jpn. J. Appl. Phys*., vol. 32, pp. 4057-4060, Sept. 1993.

[18] W. Zhahg, K. Sasaki, and T. Hata, "Low-Temperature Fabrication of Pb(Zr, Ti)O_3 Films by RF Reactive Sputtering Using Zr/Ti + PbO Target," *Jpn. J. Appl. Phys*., vol. 34, pp. 5120-5123, Sept. 1995.

[19] D. Minh, N. Loi, N. Duc, and B. Trinh, "Low-temperature PZT thin-film ferroelectric memories fabricated on SiO2/Si and glass substrates," *Journal of Science: Advanced Materials and Devices*, vol. 1, pp. 75-79, Apr. 2016.

[20] C. Cho, W. Lee, B. Yu, and B. Kim, *Journal of Applied Physics*, vol. 86, pp. 2700, 1999.

[21] S. Kim, H. Park, S. Kim, H. Wikle, J. Park, and D. Kim, "Comparison of MEMS PZT Cantilevers Based on d31 and d33 Modes for Vibration Energy Harvesting," *J. Micromech. Microeng*., vol. 22, pp. 26-33, Feb. 2013.

Un-Hyun Lim He received B.S degree in electrical and computer engineering from Ajou University. His research interests are SAW filter, untrasound and hydrogen gas sensor·

Jin-Hee Yoo He received B.S degree in electrical and computer engineering from Ajou University. His research interests are ultrasonic simulation and RF testing.

Vijay Kondalkar He received Ph.D degree in chemistry from Shivaji University. His research interests are CH_4 sensor, GMI magnetic sensor, and supercapacitor.

Keekeun Lee He received Ph.D degree in electrical and computer engineering from Arizona state University. His research interests are MEMS, sensor, SAW, holographic display.